k-asymmetric spin-splitting at the interface between transition metal ferromagnets and heavy metals

Sergiy Grytsyuk[1], Abderrezak Belabbes[1], Paul M. Haney[2], Hyun-Woo Lee[3], Kyung-Jin Lee[4,5], M. D. Stiles[2], Udo Schwingenschlögl[1],* and Aurelien Manchon[1]†

[1] *Physical Science and Engineering Division, KAUST, 23955-6900 Thuwal, Kingdom of Saudi Arabia*

[2] *Center for Nanoscale Science and Technology, National Institute of Standards and Technology, Gaithersburg, Maryland 20899-6202, USA*

[3] *PCTP and Department of Physics, Pohang University of Science and Technology, Kyungbuk 790-784, Korea*

[4] *Department of Materials Science and Engineering, Korea University, Seoul 136-713, South Korea*

[5] *KU-KIST Graduate School of Converging Science and Technology, Korea University, Seoul 136-713, Korea*

[6] *Center for Nanoscale Science and Technology, National Institute of Standards and Technology, Gaithersburg, Maryland 20899-6202, USA*

(Dated: November 19, 2015)

We systematically investigate the spin-orbit coupling-induced band splitting originating from inversion symmetry breaking at the interface between a Co monolayer and 4d (Tc, Ru, Rh, Pd, and Ag) or 5d (Re, Os, Ir, Pt, and Au) transition metals. In spite of the complex band structure of these systems, the odd-in-k spin splitting of the bands displays striking similarities with the much simpler Rashba spin-orbit coupling picture. While we do not find salient correlations between the interfacial magnetic anisotropy and the odd-in-k spin-splitting of the bands, we establish a clear connection between the overall strength of the band splitting and the charge transfer between the d-orbitals at the interface. Furthermore, we show that the spin splitting of the Fermi surface scales with the induced orbital moment, weighted by the spin-orbit coupling.

I. INTRODUCTION

The development of modern spintronic devices, such as magnetic random access memories and current-driven nano-oscillators, is currently relying on the exploitation of the mechanism of spin transfer torque[1] in magnetic systems displaying perpendicular magnetic anisotropy[2]. Besides materials displaying bulk perpendicular magnetic anisotropy (such as ordered alloys[3]), the most promising devices involve multilayers accommodating large interfacial-induced perpendicular magnetic anisotropy, such as interfaces between transition metal ferromagnets and noble metals[4] or metal oxides[5,6]. This combination has proven successful in reducing the critical current density needed to achieve current-driven magnetic excitations and switching within a reasonable range (i.e. below 10^6 A/cm^2). However, the difficulty in reducing this critical current density further constitutes a major hurdle towards applications, calling for innovative mechanisms beyond spin transfer torque. As discussed below, the physics of spin-orbit coupling at the origin of the perpendicular magnetic anisotropy might hold the key to the next technological breakthrough[7].

Interfacial perpendicular magnetic anisotropy at X/F interfaces (X being a noble metal, F a transition metal ferromagnet) is a subtle phenomenon that arises from spin-orbit coupled orbital overlaps. Spin-orbit coupling, given by $H_{\rm so} = (\xi/\hbar)\boldsymbol{\sigma}\cdot(\boldsymbol{\nabla}V\times\mathbf{p})$ (ξ is the spin-orbit coupling strength in eV/m^2), couples the spin degree of freedom $\boldsymbol{\sigma}$ to the gradient of the crystal field $\boldsymbol{\nabla}V$. In the spherical atomic potential approximation, $\boldsymbol{\nabla}V \propto \mathbf{r}$ and the interfacial perpendicular magnetic anisotropy is conventionally associated with the orbital overlap leading to an enhanced interfacial orbital angular momentum $\mathbf{L} = \mathbf{r}\times\mathbf{p}$[4,8,9]. In the independent ligand theory, its magnitude can be related to the anisotropy of the orbital angular momentum $\Delta E_{\rm so} = \xi/(4\mu_{\rm B})(m_{\rm orb}^{\parallel} - m_{\rm orb}^{\perp})$[4,10], where $m_{\rm orb}^{\parallel(\perp)}$ is the orbital moment when the magnetization lies in (perpendicular to) the plane and $\mu_{\rm B}$ is the Bohr magnetron. Since the anisotropy in orbital momentum is driven by spin-orbit coupling, in this simple scenario (which disregards the complexity of interfacial orbital overlaps) the interfacial perpendicular magnetic anisotropy is then second order in spin-orbit coupling strength ξ. Therefore, interfacial perpendicular magnetic anisotropy survives in symmetrically grown systems such as Pt/Co/Pt, for instance. However, when the two interfaces embedding the transition metal ferromagnet are not equivalent, such as in Pt/Co/AlOx or Ta/CoFeB/MgO, the symmetry is broken and additional effects emerge.

In such systems, the sharp interface between the ferromagnet and the noble metal breaks the inversion symmetry along the normal to the interface, $\mathbf{z}$. In a simplistic picture, the gradient of potential becomes $\langle\xi\boldsymbol{\nabla}V\rangle \approx -\alpha\mathbf{z}$ and the spin-orbit coupling Hamiltonian reduces to $H_{\rm R} \approx -\alpha\boldsymbol{\sigma}\cdot(\mathbf{z}\times\mathbf{k})$, where α is the so-called Rashba parameter[11,12]. Such $\mathbf{k}$-linear spin-orbit coupling has been observed at the surface of various metals such as Au[13], Gd[14], or Bi compounds[15,16] and more recently at the surface of three dimensional topological insulators[17]. Notice that in general, spatial inversion symmetry breaking imposes the spin-orbit coupling term to be *odd* in momentum $\mathbf{k}$, but not necessarily linear. Indeed, such odd-in-k spin-orbit coupling is well known in bulk non-centrosymmetric semiconductors[18] and has been detected recently at oxide heterointerfaces[19].

A direct consequence of this odd-in-k spin-orbit coupling on the local spin configuration is the emer-

gence of an antisymmetric exchange interaction, the so-called Dzyaloshinskii-Moriya interaction[20], on the form $\sum_{ij} \mathcal{D}_{ij} \mathbf{S}_i \times \mathbf{S}_j$ where $\mathbf{S}_{i(j)}$ is the direction of the spin angular momentum of the ion at position $\mathbf{r}_{i(j)}$. Under certain conditions (exchange, anisotropy, temperature etc.), this interaction produces chiral spin textures such as spin spirals, as observed at W/Mn and Ir/Fe interfaces[21,22], and skyrmions[23]. Very recently, it has also been shown that this interaction favors Néel over Bloch configuration of magnetic domain walls in Ni/Fe multilayers[24]. Such a distortion is a key element to understand the observed anomalous domain wall motion in ultrathin perpendicularly magnetized multilayers[25,26].

Another important phenomenon that may play a role in materials lacking inversion symmetry is the current-driven spin-orbit torque[27]. In non-centrosymmetric multilayers, the interfacial odd-in-k spin-orbit coupling enables the so-called inverse spin galvanic effect, i.e. the electrical generation of a non-equilibrium spin density[28]. This spin density can be used to manipulate the magnetization of the adjacent ferromagnet. Spin-orbit torque has been theoretically predicted using model Hamiltonians with Rashba or Dresselhaus spin-orbit coupling[29,30] and first principle calculations on realistic interfaces have been achieved recently[31], confirming qualitatively the theoretical results. Its experimental identification in Pt/Co/AlOx[32,33] and other similar structures[34,35] is currently a growing field in spin electronics and regarded as a possible way to complement or even replace spin transfer torque in devices possessing perpendicular magnetic anisotropy.

While these phenomena all arise from interfacial symmetry breaking in the presence of spin-orbit coupling, the details of these mechanisms remain quite complex and explicit connections have only been established within the framework of Rashba spin-orbit coupling[36]. Indeed, first principle calculations clearly revealed that this latter approximation is far from realistic[31,37–39]: Breaking spatial inversion symmetry hardly affects the strength of the atomic spin-orbit coupling itself (in sharp contrast with the phenomenological picture developed by Bychkov and Rashba[11]), but it distorts the wave function close to the nuclei, where the spin-orbit coupling is stronger[37–39]. The interaction between atomic spin-orbit coupling and these distorted wave functions results in an effective odd-in-k spin-orbit coupling. In addition, in metallic systems the detail of the orbital hybridization at the interface between, say, a ferromagnet and a heavy metal is quite complex, resulting in an induced magnetic moment in the heavy metal and an enhancement of the orbital momentum in the ferromagnet. Providing a clear description of the interfacial spin-orbit coupling-induced band splitting and associated phenomena for a wide variety of materials could help designing interfaces with tunable properties.

In this article, in order to uncover the physics governing the interfacial spin-orbit coupling in such bilayers, we present a systematic investigation of the (spin-orbit coupling-induced) band splitting at X/Co interfaces, where X represents a $4d$ or $5d$ metal as depicted in Fig. 1. Using first principle methods, we establish clear connections between the odd-in-k spin splitting and the interfacial orbital angular momentum and related charge transfer. This article is organized as follows. Computational details are summarized in Section II and the results are reported in Section III. Section III A presents the electronic structure of these interfaces together with their magnetization profile, while Section III B describes the spin-orbit coupling-induced band splitting properties. A summary is given in Section IV.

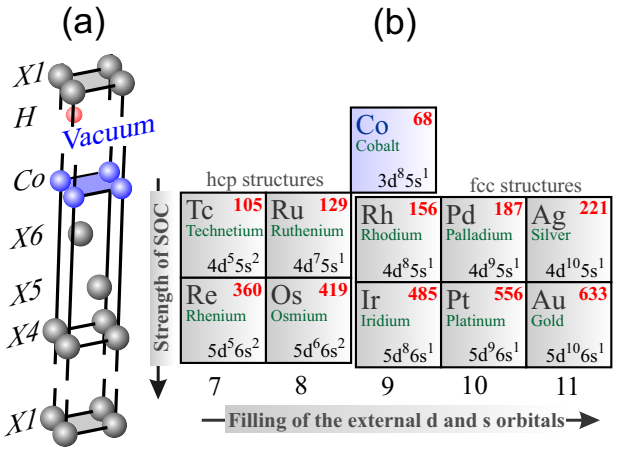

FIG. 1: (a) Structure of the X/Co interfaces (X= $4d$-metals = Tc, Ru, Rh, Pd, Ag and X = 5d-metals = Re, Os, Ir, Pt, Au) and (b) their electronic configurations used in this work[41]. Numbers in red stand for the strength of spin-orbit coupling in meV.

II. COMPUTATIONAL DETAILS

In principle, the accurate description of the magnetic and electronic properties of X/Co interfaces (X = $4d$- and X= $5d$-metals) using first principles calculations necessitates the definition of a huge supercell in $\widehat{xy}$ plane with Moiré pattern[40] due to the large lattice mismatch between the two materials. However, the large size of the cell combined with the presence of spin-orbit coupling makes such calculations computationally expensive. To avoid this hurdle, we imposed the lattice parameter of the free standing Co layer to match the lattice parameter of the substrate X. Due to the artificial strain, the computed electronic and magnetic properties of the X/Co system may be different from the ones of a realistic interface. Indeed, in Ref.[40] it was demonstrated that for a Co monolayer deposited on top of Pt (Au), the tensile stress results in an enhancement of the magnetic moments of Pt (Au) and Co layers by 22 % (10 %) and 10 % (15 %), respectively. The objective of the present work is not to match the experimental observations by modeling a realistically disordered interface but rather to describe the systematic modification of the band splitting and mag-

netic properties of such bilayers when changing the heavy metal substrate.

In this work, a monolayer of Co was placed on top of a 6-layer slab of a X(111) substrate that is either a 4d (Tc, Ru, Rh, Pd, and Ag) or a 5d metal (Re, Os, Ir, Pt, and Au), see Fig. 1(a). This allows us to study the dependence of the band splitting and its related properties as a function of the spin-orbit coupling strength and electronic configurations of the external ds-orbitals, as illustrated in Fig. 1(b). Moving from the left to the right side of the table, the number of electrons on the external ds-orbitals grows from 7 to 11. Structures with $[ds]^7$ and $[ds]^8$ electronic configurations have hcp packing while with $[ds]^9$, $[ds]^{10}$ and $[ds]^{11}$ electronic configurations adopt fcc packing. Our test calculations reveal that Co prefers hcp and fcc hollow sites on top of X in the first and second cases, respectively. In addition, a vacuum of 10 Å and one H atom on the bottom of the substrate were found as sufficient conditions to avoid charge accumulation. First principle calculations were performed in the generalized gradient approximation[42]. For the structure optimization we used the pseudopotential method that is implemented in VASP[43,44 56] while the magnetic properties were investigated within the full-potential code FLEUR[45]. The magnetic properties were calculated using an increased number of k-points in the Brillouin zone until convergence which is achieved for 2304 k-points. To study the band splitting below and at the Fermi level we used 256 k-points for each radial direction and 4096 equally-distributed k-points in the irreducible Brillouin zone, respectively.

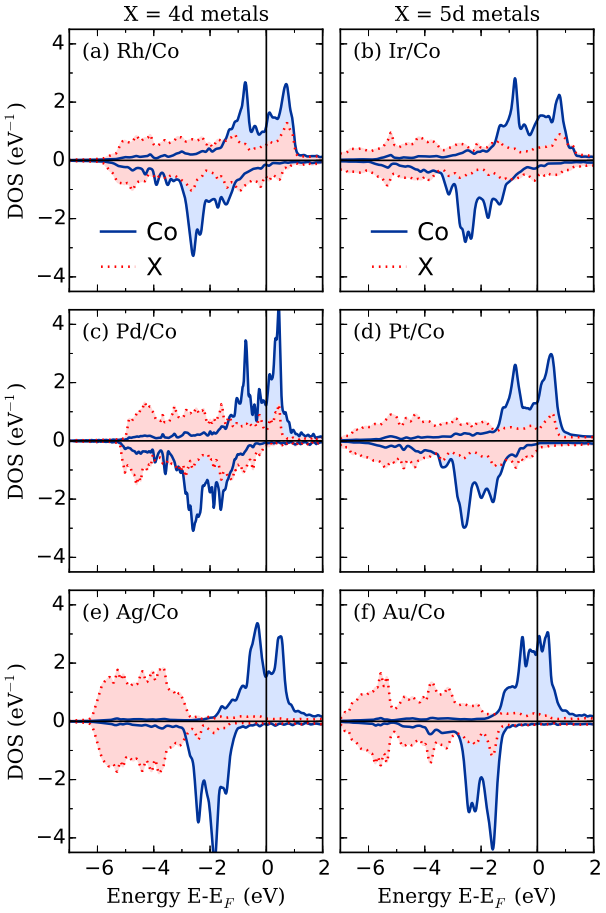

FIG. 2: Projected density of states (DOS) for the X/Co interfaces, where X is a heavy metal as indicated on the figure. The amount of hybridization between the 3d orbitals of Co and 4(5)d orbitals of the heavy metal decreases when increasing the d-orbital filling of the heavy metal. The densities of states for X=Tc, Ru, Re and Os are not represented as they show a qualitatively similar behavior as heavy metals with partially filled d-shells.

III. RESULTS AND DISCUSSION

A. Electronic structures

The magnetic properties of X/Co interfaces are direct outcomes of interfacial orbital overlap. Therefore, before entering in the detailed analysis of these properties, we turn our attention towards the nature of these hybridizations. The density of states and magnetic properties of the d-orbitals of X/Co bilayers are displayed in Figs. 2 and 3, respectively. The first remarkable feature is the distinct behavior between metals with partially filled d-shells (Tc, Ru, Re, Os, Ir, Pt, Rh and Pd) and metals with filled d-shells (Au and Ag). While the formers present a sizable density of states at the Fermi energy, this density of states is vanishingly small in the latter cases. As a consequence, the hybridization between Co and X strongly depends on the d-orbital filling. Indeed, upon increasing the d-orbital filling, the binding energy decreases due to (i) the enhancement of the "artificial" lattice distortion imposed by the lattice mismatch between Co and X and (ii) the reduction of the orbital hybridization. The latter results in a strong reduction of the Co-X binding in the case of Au and Ag.

The nature of the orbital hybridization between Co and X has important consequences on the magnetic properties at the interface. First, metals with partially filled d-shells acquire a large magnetic moment through proximity effect[8,46–48], which vanishes in the case of metals with filled d-shells (Au and Ag). Notice that the magnetic proximity effect is very small in the case of Tc, Ru, Os and Re but does not vanish. Most importantly for the present study, the magnetic proximity effect is accompanied by an induced orbital moment that is negative for Tc, Ru, Re, and Os and positive at the interface with Rh, Pd, Ag, Ir, Pt, and Au, see Fig. 3(b). As discussed below, the sign and magnitude of the induced orbital moment has a dramatic impact on the spin-orbit-induced splitting of the band structure.

It is worth mentioning that all the structures discussed in this work and involving heavy metals with partially-filled d-shells present interfacial perpendicular magnetic anisotropy, while the weak hybridization between Co and

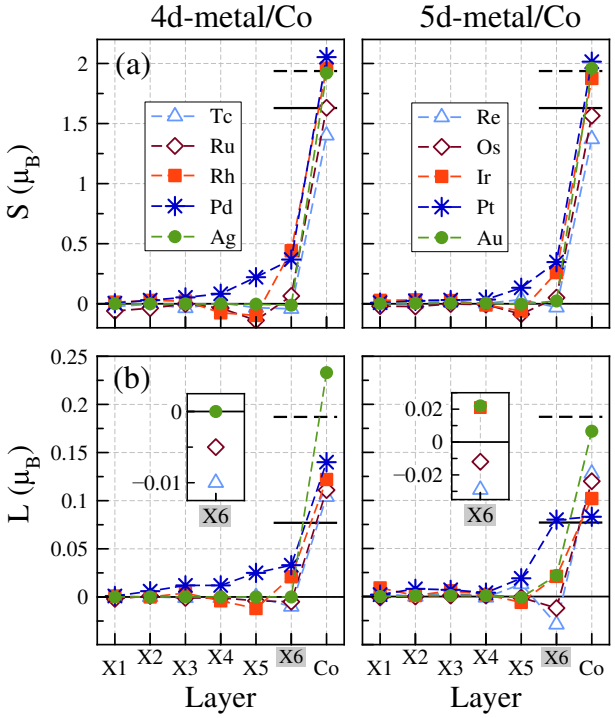

FIG. 3: Layer resolved magnetic properties of the X/Co interfaces, where X is a heavy metal. (a) spin and (b) orbital contributions to the magnetic moment for a magnetization pointing along **x**. The left (right) panels represent the 4*d* (5*d*) metals, as indicated on the figure. Solid (dashed) line indicates the value for the bulk (free standing layer of) Co.

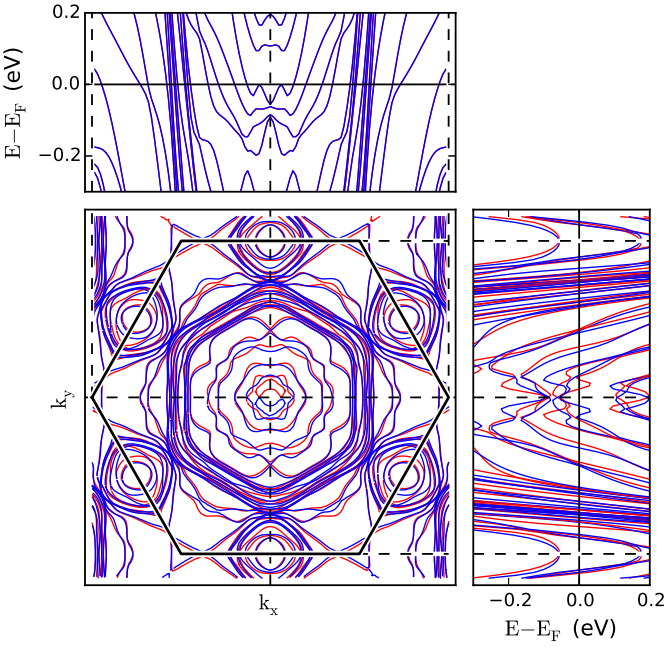

FIG. 4: (Color online) Central panel: two-dimensional Fermi surface of Ir/Co interface in (k_x, k_y) plane, when the magnetization direction is along $+\mathbf{x}$ (red lines) or $-\mathbf{x}$ (blue lines). Right panel: Band structure of Ir/Co interfaces calculated along the y-direction in Brillouin zone; Top panel: Band structure of Ir/Co interfaces calculated along the x-direction in Brillouin zone. A clear splitting of the band structure is observed when the band structure is projected perpendicular to the magnetization direction (Right panel), while no splitting appears when the band structure is projected along the magnetization direction (Top panel).

metal with filled *d*-orbitals (Ag and Au) results in large in-plane magnetic anisotropy[48–50]. However, since we could not find any robust correlation between the magnetic anisotropy and the strength of the band splitting, we choose not to further discuss magnetic anisotropy here.

B. *k*-asymmetric spin splitting

In the previous section, we have illustrated the complex hybridization scheme of heavy metal/ferromagnet interfaces through the onset of magnetic proximity effect as well as induced orbital moment. We now turn our attention towards the main topic of the present work, i.e. the nature of spin-orbit coupling-induced spin-splitting in asymmetric magnetic bilayers.

1. *Spin-orbit induced band splitting*

In inversion asymmetric systems, spin-orbit coupling induces a spin-splitting of the band structure on the form $H_{\rm so} = \mathbf{w}(\mathbf{k}) \cdot \boldsymbol{\sigma}$, where $\mathbf{w}(\mathbf{k}) = -\mathbf{w}(-\mathbf{k})$ is an odd function of $\mathbf{k}$. In order to visualize and analyze such a band splitting, we adopt the approach developed in Ref. 51: The band structure is calculated for two opposite directions of the magnetization, say $\pm\mathbf{u}$, hence revealing the spin-orbit coupling-induced asymmetric spin-splitting. For instance, the Fermi surface and band structures of the Ir/Co interface along the x- and y-directions in Brillouin zone is reported on Fig. 4, central, top, and right panels, respectively, when imposing the magnetization to lie along $+\mathbf{x}$ (red lines) and -**x** (blue lines). The band structures obtained for opposite magnetization directions are mirror symmetric with respect to $k_y = 0$, as expected, ensuring that the band structure remains time-reversal symmetric, i.e. $\delta E(m_x, k_y) = \delta E(-m_x, -k_y)$. When the magnetization is applied along $\pm\mathbf{x}$, the band structure calculated along the x-direction in Brillouin zone does not display any spin-splitting, see Fig. 4 top panel. Similar results have been obtained for all the substrates considered. When removing the interface, using either an isolated Co or X layer, this asymmetric splitting disappears (not shown).

Evaluating the strength of the odd-in-k spin-splitting has been achieved using various approaches. For instance, Bihlmayer *et al.*[37] directly calculated the potential gradient $\langle \partial_r V/r \rangle$ close to the atom nucleus, Park *et al.*[51] evaluated the linear slope of the band structure close

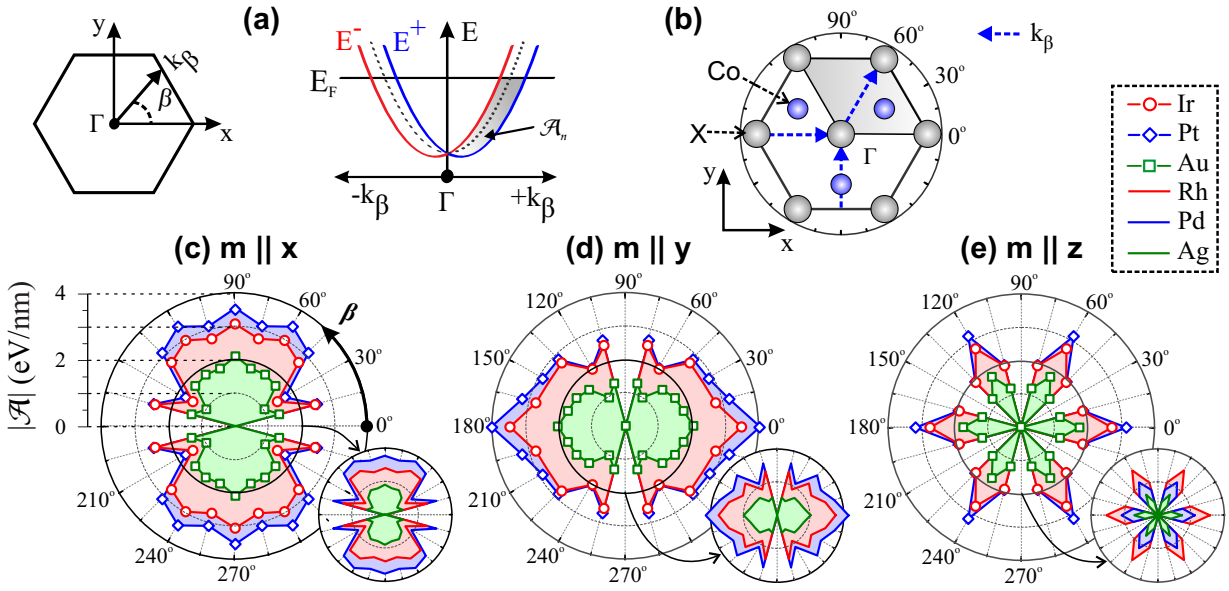

FIG. 5: (a) Brillouin zone and schematic representation of the odd-in-k splitting along β direction. $\mathcal{A}_n$ is the spanned area; (b) (x,y)-projection of the X/Co interface. k_β are examples of the electron propagation directions with respect to the crystal structure; (c), (d), and (e) $|\mathcal{A}| = |\mathcal{A}(\beta)|$, for the magnetization along $+\mathbf{x}$, $+\mathbf{y}$, and $+\mathbf{z}$ directions, respectively. Small and large polar coordinates have the same scale and refer to the 4d-metal/Co and 5d-metal/Co interfaces, respectively. For the sake of readability, the value of $|\mathcal{A}|$ for Tc, Ru, Os and Re are omitted in this figure.

to $k = 0$ (which probably corresponds to the closest definition of the Rashba spin-splitting), while Haney *et al.*[31] calculated the inverse spin galvanic effect arising from odd-in-k spin splitting (which is a more experimentally-relevant quantity). The variety of methods illustrates the difficulty to give a proper account of the strength of spin-orbit coupling-induced spin-splitting in asymmetric systems. In the present work, we adopt an intuitive approach to evaluate the magnitude of the spin-splitting at and below the Fermi level.

2. *Spin-splitting below Fermi level*

The area spanned by the band n upon magnetization reversal from $+\mathbf{u}$ to $-\mathbf{u}$ is $\mathcal{A}_n = \int |E_n^+ - E_n^-| dk$ [shaded area in Fig. 5(a)], where $E_n^\pm$ is the energy dispersion when the magnetization lies along $\pm\mathbf{u}$. To evaluate the global strength of the spin splitting below the Fermi level, we calculate the total area $\mathcal{A}$ as

$$|\mathcal{A}| = \sum_n^N \sum_i^{N_k} |\Delta E_{ni}| \Delta k_i, \qquad (1)$$

where the first summation $\sum_n^N$ runs over the band index n, the second summation $\sum_i^{N_k}$ stems from the discretization of the integral in k-space and $\Delta E_{ni} = E_{ni}^+ - E_{ni}^-$. Notice that in Eq. (1) only absolute values of the energy shifts enter the calculation. Indeed, since the sign of the spin-splitting depends on the band index[51] accounting for the relative magnitudes of the shifts rather than for their absolute values would result in cancellations between different bands and might not give a full account of the global spin splitting strength. By calculating the absolute value of $|\mathcal{A}|$, we ensure that we evaluate only the absolute strength of the asymmetric spin-splitting. Therefore $|\mathcal{A}|$ provides an estimation of the spin-splitting asymmetry for all bands below the Fermi energy.

In contrast to systems that have a well-isolated surface state [such as Au (111) surface[13] or Bi/Ag (111) surface alloy[15]], in case of X/Co bilayers the strong interfacial spin-orbit splitting is spread over the continuum of bulk bands. However, since $|\mathcal{A}|$ is determined by the states close to the interface, its magnitude converges quickly as the thickness of the substrate increases, as shown on Figs. 6 (a) and (b). To numerically compute $|\mathcal{A}|$, the band structure calculations were repeated for different directions β in the Brillouin zone [see Fig. 5(a)], as well as for three different magnetization directions (along $\mathbf{x}$, $\mathbf{y}$ and $\mathbf{z}$ axes). The spanned absolute areas $|\mathcal{A}|$ calculated for various β directions in the Brillouin zone and when the magnetization lies along $\mathbf{x}$, $\mathbf{y}$ and $\mathbf{z}$ axes are shown on Fig. 5 (c), (d) and (e), respectively. Several features are worth noticing.

First, while the global angular dependence of $|\mathcal{A}|$ depends on the magnetization direction and displays different symmetries in the different cases, their shapes do not depend on the substrate. Second, when the magnetization lies in the interface plane $(\mathbf{x}, \mathbf{y})$, $|\mathcal{A}|$ reaches its maximum when the $\mathbf{m}\perp\mathbf{k}$ ($\beta = \pm 90°$ when $\mathbf{m}||\mathbf{x}$ and $\beta = 0°$ when $\mathbf{m}||\mathbf{y}$) and vanishes when $\mathbf{m}||\mathbf{k}$ ($\beta = 0°$ when $\mathbf{m}||\mathbf{x}$ and $\beta = \pm 90°$ when $\mathbf{m}||\mathbf{y}$). This partially ascertains a standard Rashba model described by the Hamiltonian

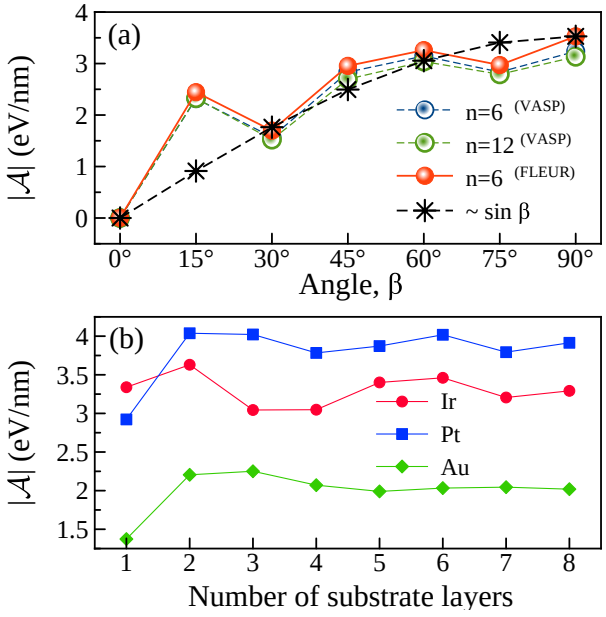

FIG. 6: (a) Angular dependence of the total band splitting $|\mathcal{A}(\beta)|$ calculated by first principles (VASP and FLEUR) and by the standard Rashba model ($H_{\rm R} \propto \sin\beta$ - see main text) for the Pt_n/Co interfaces (n is a number of Pt layers). Magnetization is along **x**. (b) Dependence of $|\mathcal{A}(\beta = 0°)|$ on the number of substrate layers for Ir, Pt, and Au. Magnetization is along **y**.

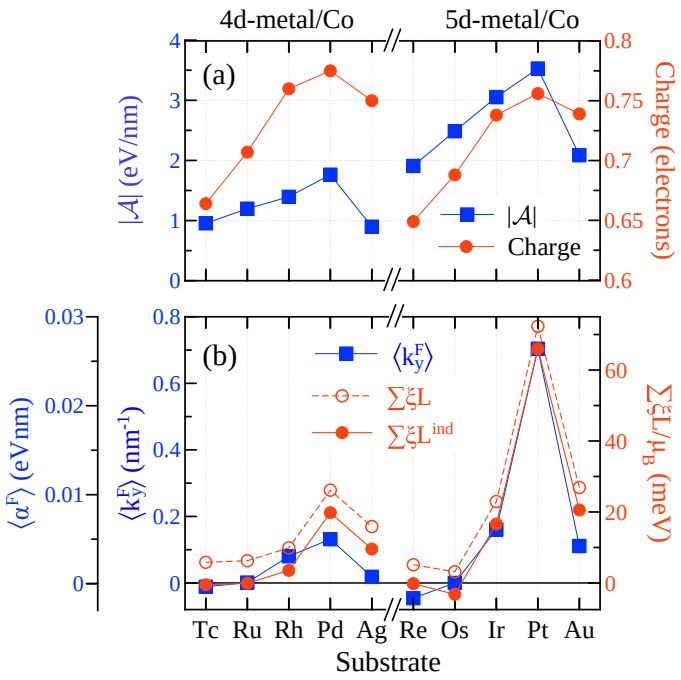

FIG. 7: Correlation between odd-in-k spin splitting and interfacial electronics properties as a function of substrate: (a) spanned area $|\mathcal{A}|$ (blue symbols) and charge transfer from the d-orbitals of substrate to the d-orbitals of Co (red symbols); (b) effective momentum shift $\langle k_y^{\rm F}\rangle$ (blue symbols) and summation of the induced orbital moments of each atom weighted by their spin-orbit coupling constant, $\sum_i \xi_i L_i^{ind}$ (red symbols).

$H_{\rm R} = \alpha(\boldsymbol{\sigma}\times\mathbf{k})\cdot\mathbf{z} \propto \sin\beta$. Fig. 6(a) compares the angular dependence of the magnitude of $|\mathcal{A}|$ extracted from the first principle calculations (from both VASP and FLEUR codes) reported on Fig. 5(c) and the expected $\sin\beta$ dependence. Deviations from the sine shape are clearly visible at β=15°, 45°, and 75°, which correspond to points where the in-plane crystalline symmetry is broken, see Fig. 5(b). Notice that these calculations have been reproduced for a thicker substrate thickness [n=12 layers, green symbols in Fig. 6(a)] with only minor variations, showing that $|\mathcal{A}|$ is a robust quantity to characterize the total band splitting below the Fermi level. Third, a spin-splitting is observed when the magnetization lies out of the plane of the interface [see Fig. 5(e)]. In fact, the spin-splitting in this case displays a 6-fold symmetry which is a reminiscence of the crystal structure [see Fig. 5(c)]. The vanishing splitting at $\beta = 30° + m\times 60°$, $m \in \mathbb{Z}$, corresponds to high symmetry points in Brillouin zone while the maxima at $\beta = m\times 60°$ corresponds to low symmetry points [see Fig. 5(b)]. Of course, in a system with cylindrical symmetry around **z** like in a two-dimensional free electron gas with Rashba spin-orbit coupling, no splitting is observed when the magnetization lies along **z**.

Finally, one can notice that the magnitude of $|\mathcal{A}|$ also depends strongly on the substrate as reported on Fig. 7(a). Generally, 4d substrates display weaker spin splitting than 5d substrates, which is a direct consequence of their weaker spin-orbit coupling strength. However, the spin splitting magnitude also depends on the band filling and within a same class of materials (either 4d or 5d) shows a maximum for n$[ds]^{10}$ materials (i.e. Pd and Pt), see Fig. 1. As mentioned in the introduction, Bihlmayer *et al.*[37] and more recently Krasovskii[53] have noticed that, in contrast with the conventional phenomenology of Rashba spin-orbit coupling, the interfacial symmetry breaking leaves the atomic spin-orbit coupling unaffected while it strongly distorts the wave function itself. The interplay between this distorted wave function and the spherically symmetric spin-orbit coupling produces the asymmetric spin splitting of the band structure. The distortion of the wave function at the interface between the substrate and the Co monolayer is associated with a charge transfer from the substrate to the Co layer, which is reported on Fig. 7(a) for d-orbitals. A qualitative correlation is obtained between the spin splitting parameter $|\mathcal{A}|$ and the charge transfer, both displaying a maximum for Pd and Pt.

3. *Spin splitting at the Fermi level*

Let us now turn our attention towards the properties of the Fermi surface, displayed in Fig. 4, central panel, for Ir/Co. While the Fermi surface is very far from circular, it displays a shift along the y-direction when changing

the magnetization direction from +**x** (red) to -**x** (blue), confirming the intuition given by the Rashba model. To evaluate the strength of the spin splitting at the Fermi level, we compute the k-averaged Fermi wave vector $\langle \mathbf{k}^F \rangle$ defined

$$\langle \mathbf{k}^F \rangle = \sum_n^{N_b} \mathbf{k}_n^F = \sum_n^{N_b} \frac{1}{N_k} \sum_i^{N_k} \mathbf{k}_{in}^F, \qquad (2)$$

where the first summation $\sum_n^{N_b}$ runs over the band index n and second one $\sum_i^{N_k}$ stems from the discretization of the integral in k-space. If there is no spin splitting, $\langle \mathbf{k}^F \rangle = 0$. In the present case, the magnetization is along $\pm\mathbf{x}$ so that $\langle \mathbf{k}^F \rangle = \langle k_y^F \rangle \mathbf{y}$, as in Fig. 4. The physics behind this term is quite subtle. The velocity operator is $\mathbf{v} = \partial_{\mathbf{k}} H/\hbar$, which reduces to $\mathbf{v} = \mathbf{k}/m$ in the free electron model in the *absence* of spin-orbit coupling. Therefore, $\langle k_y^{\mathrm{F}} \rangle$ is a partial measure of the spin galvanic effect induced by the symmetry breaking revealed when the magnetization lies away from a high symmetry direction. Notice that $\langle k_y^{\mathrm{F}} \rangle$ is *not* the total spin galvanic effect, which should contain the anomalous velocity term (proportional to the non-equilibrium spin density) and vanishes at equilibrium. The calculated $\langle k_y^{\mathrm{F}} \rangle$ is reported on Fig. 7(b) for different substrates. While it is quite small in the case of 4d metals, it is much larger for 5d metals. In both cases maximum is reached for $[ds]^{10}$ configurations, that corresponds to Pd and Pt substrates.

Since the electronic states at the Fermi level are delocalized, they are more likely to be affected by the interfacial potential gradient $\nabla_z V$ due to the charge transfer. The charge transfer scales with the strength of the orbital hybridization, and results in an enhancement of the orbital angular momentum on the substrate as reported on Fig. 3(b). Park *et al.*[52] proposed that at a surface, the local orbital momentum in the presence of surface normal electric field (due to inversion symmetry breaking) results in Rashba-type splitting. Following this idea, we assume that the strength of the band splitting for the X/Co bilayers should be proportional to $\sum_i \xi_i L_i$, where L_i and ξ_i, are atomic orbital moment [Fig. 3(b)] and spin-orbit coupling constant [Fig. 1(b)], respectively, in each layer i. The quantity $\sum_i \xi_i L_i$ for the X/Co interfaces is displayed on Fig. 7(b) (open red symbols) and shows good correlation with $\langle k_y^{\mathrm{F}} \rangle$. However, $\sum_i \xi_i L_i$ is shifted with respect to $\langle k_y^{\mathrm{F}} \rangle$ and is always positive while $\langle k_y^{\mathrm{F}} \rangle$ reaches negative values for some of the X/Co interfaces. We find that this shift can be eliminated by replacing the total orbital moment L_i by the *induced* orbital moment $L_i^{ind} = L_i - L_i^{bulk}$, where L_i^{bulk} is the value of the orbital momentum in the bulk of layer i (either bulk X or bulk Co). Quantity $\sum_i \xi_i L_i^{ind}$ is displays on Fig. 7(b) (filled red symbols) and shows an excellent correlation with $\langle k_y^{\mathrm{F}} \rangle$, i.e. $\langle k_y^{\mathrm{F}} \rangle \approx \eta \sum_i \xi_i L_i^{\mathrm{ind}}$, where $\eta\mu_B \approx 10.7$ (eVnm)$^{-1}$ (calculated in this work). Thus, the presence of the induced orbital moment is a necessary condition for the onset of k-asymmetric band splitting.

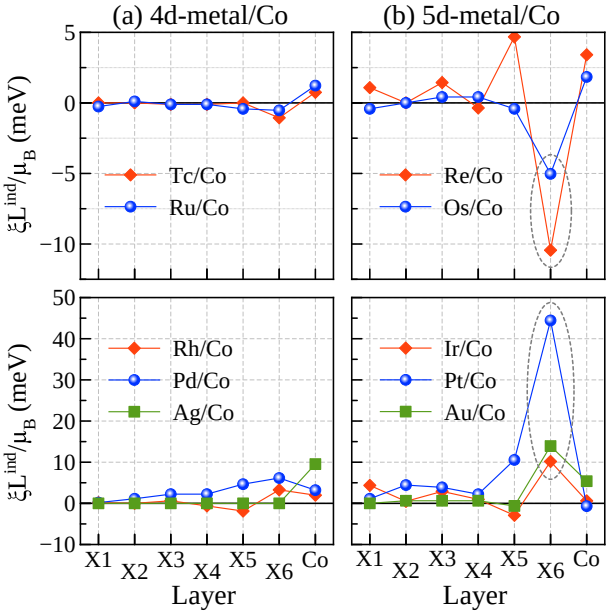

FIG. 8: Induced orbital moment weighted by spin-orbit coupling for: (a) 5d-metal/Co and (b) 4d-metal/Co interfaces. Induced orbital moment for each i is $L_i^{ind} = L_i^{X/Co} - L_i^{bulk}$.

In order to complete our description of the physics involved, we present the layer contribution of $\xi_i L_i^{\mathrm{ind}}$ in Fig. 8. First we note that the substrate contribution to the band splitting is large in the case of 5d-metals while in the case of 4d-metals it is comparable with Co contribution. For instance, at the Ag/Co interface, Ag is not magnetized ($L_{Ag}^{ind} = 0$) thus the main contribution comes from Co. At the Pd/Co interface in contrast, the induced orbital momentum of Pd does not vanish away from the interface [see Fig. 3(b)]. Thus Pd/Co interface has the largest strength of the band splitting among other 4d-metal/Co interfaces [see Fig. 7(b)]. Regarding 5d-metal/Co interfaces, the largest $\xi_i L_i^{\mathrm{ind}}$ is observed at the Pt/Co interface, associated with a large induced orbital momentum [see Fig. 3(b)]. Moreover, one can see from Fig. 8, that the induced orbital momentum of $[ds]^{7-8}$ substrates (Tc, Ru, Re, and Os) is negative while it is positive in the case of $[ds]^{8-10}$ substrates (Rh, Pd, Ag, Ir, Pt, and Au). This nicely correlated with the sign of $\langle k_y^{\mathrm{F}} \rangle$ for the X/Co interfaces reported in Fig. 7(b).

We conclude this study by evaluating the effective Rashba parameter resulting from the k-asymmetric band splitting. Although the band structure of X/Co bilayers is much more complex than the free electron model, the Rashba parameter is commonly used in experiments to quantify non-equilibrium properties related to interfacial spin-orbit coupling such as inverse spin galvanic effect. The Rashba parameter at Fermi energy $\langle \alpha^F \rangle$ can be connected with the parameter $\langle k^F \rangle$ defined in Eq. (2),

$$\langle \alpha^F \rangle = \frac{\hbar^2}{2} \sum_n^{N_b} \frac{1}{N_k} \sum_i^{N_k} \frac{k_{ni}^F}{m_{ni}^*} \approx \frac{\hbar^2}{2m_e} \langle k^F \rangle. \qquad (3)$$

The result is shown on Fig. 7(b), assuming the same free electron effective mass $m^* = m_e$ for all systems. The largest Rashba parameter is obtained for Pt/Co ($\langle\alpha^F\rangle_{\rm Pt} \approx 25 \times 10^{-3}$ eV nm) while Ir/Co, Au/Co and Pd/Co have a much smaller parameter ($\approx 5 \times 10^{-3}$ eV nm). These values are smaller than the one reported in Ref. 51 for Pt/Co ($\approx 100 \times 10^{-3}$ eV nm). These estimations must be handled with sane skepticism (in realistic metals, $m^* \ll m_e$, and lattice distortions are disregarded in our calculations) but can be compared with the effective parameters extracted experimentally from current-driven field measurements, i.e. 100 $\times 10^{-3}$ eV nm for Pt/Co[32], and 36 $\times 10^{-3}$ eV nm for Pd/Co/Pd asymmetric interfaces[34].

IV. DISCUSSION AND CONCLUSION

In this work, we systematically studied the band splitting originating from spatial inversion symmetry breaking in the presence of spin-orbit coupling in transition metal bilayers involving 4*d* (Tc, Ru, Rh, Pd, and Ag) and 5*d* (Re, Os, Ir, Pt, and Au) heavy metals, capped by a monolayer of Co. In spite of the complex band structure of these systems, the *k*-asymmetric spin splitting displays remarkable similarities with the much simpler Rashba model, such as the overall angular variation of the splitting (Fig. 6). Moreover, our study reveals the crucial role of interfacial orbital overlap in the onset of *k*-asymmetric spin splitting and a phenomenological correlation between the splitting strength and the spin-orbit coupling-weighted induced orbital momentum as well as *d*-orbital charge transfer (Fig. 7). Nonetheless, our results also emphasize the limits of the Rashba scenario in crystalline systems involving strong interfacial orbital overlaps. Indeed, the *k*-asymmetric spin splitting is in general *not linear* in k and depends on the band index, and spin splitting is also obtained when the magnetization lies perpendicular to the interface, due to in-plane crystalline symmetry breaking, see Fig. 5(d).

* Electronic address: udo.schwingenschlogl@kaust.edu.sa
† Electronic address: aurelien.manchon@kaust.edu.sa

[1] J. C. Slonczewski, J. Magn. Magn. Mater. **159**, L1 (1996); L. Berger, Phys. Rev. B **54**, 9353 (1996).
[2] H. Yoda, T. Kishi, T. Nagase, M. Yoshikawa, K. Nishiyama, E. Kitagawa, T. Daibou, M. Amano, N. Shimomura, S. Takahashi, T. Kai, M. Nakayama, H. Aikawa, S. Ikegawa, M. Nagamine, J. Ozeki, S. Mizukami, M. Oogane, Y. Ando, S. Yuasa, K. Yakushiji, H. Kubota, Y. Suzuki, Y. Nakatani, T. Miyazaki, and K. Ando, Curr. Appl. Phys. **10**, E87 (2010).
[3] T. Seki, S. Mitani, K. Yakushiji, and K. Takanashi, Appl. Phys. Lett. **88**, 172504 (2006).
[4] D. Weller, Y. Wu, J. Stöhr, M. G. Samant, B. D. Hermsmeier, and C. Chappert, Phys. Rev. B **49**, 12888 (1994).
[5] S. Monso, B. Rodmacq, S. Auffret, G. Casali, F. Fettar, B. Gilles, B. Dieny, and P. Boyer, Appl. Phys. Lett. **80**, 4157 (2002); B. Rodmacq, A. Manchon, C. Ducruet, S. Auffret, and B. Dieny, Phys. Rev. B **79**, 024423 (2009).
[6] S. Ikeda, K. Miura, H. Yamamoto, K. Mizunuma, H. D. Gan, M. Endo, S. Kanai, J. Hayakawa, F. Matsukura, and H. Ohno, Nature Mater. **9**, 721 (2010).
[7] A. Manchon, H.C. Koo, J. Nitta, S. Frolov, R.A. Duine, Nature Mater. **14**, 871 (2015).
[8] N. Nakajima, T. Koide, T. Shidara, H. Miyauchi, H. Fukutani, A. Fujimori, K. Iio, T. Katayama, M. Nyvlt, and Y. Suzuki, Phys. Rev. Lett. **81**, 5229 (1998).
[9] G. H. O. Daalderop, P. J. Kelly, and M. F. H. Schuurmans, Phys. Rev. B **50**, 9989 (1994).
[10] P. Bruno, Phys. Rev. B **39**, 865 (1989); J. Stöhr, J. Magn. Magn. Mater. **200**, 470 (1999).
[11] Yu A. Bychkov and E. I. Rashba, J. Phys. C: Solid State Phys. **17**, 6039 (1984).
[12] L. Petersen and P. Hedegård, Surf. Sci. **459**, 49 (2000).
[13] S. LaShell, B. A. McDougall, and E. Jensen, Phys. Rev. Lett. **77**, 3419 (1996); H. Cercellier, C. Didiot, Y. Fagot-Revurat, B. Kierren, L. Moreau, D. Malterre, and F. Reinert, Phys. Rev. B **73**, 195413 (2006).
[14] O. Krupin, G. Bihlmayer, K. Starke, S. Gorovikov, J. E. Prieto, K. Döbrich, S. Blügel, and G. Kaindl, Phys. Rev. B **71**, 201403(R) (2005).
[15] C. R. Ast, J. Henk, A. Ernst, L. Moreschini, M. C. Falub, D. Pacilé, P. Bruno, K. Kern, and M. Grioni, Phys. Rev. Lett. **98**, 186807 (2007); A. Takayama, T. Sato, S. Souma, and T. Takahashi, Phys. Rev. Lett. **106**, 166401 (2011).
[16] I. Gierz, B. Stadtmüller, J. Vuorinen, M. Lindroos, F. Meier, J. Hugo Dil, K. Kern, and C. R. Ast, Phys. Rev. B. **81**, 245430 (2010).
[17] D. Hsieh, D. Qian, L. Wray, Y. Xia, Y. S. Hor, R. J. Cava, and M. Z. Hasan, Nature **452**, 970 (2008); Y. L. Chen, J. G. Analytis, J.-H. Chu, Z. K. Liu, S.-K. Mo, X. L. Qi, H. J. Zhang, D. H. Lu, X. Dai, Z. Fang, S. C. Zhang, I. R. Fisher, Z. Hussain, and Z. -X. Shen, Science **325**, 178 (2009).
[18] G. Dresselhaus, Phys. Rev. **100**, 580 (1955).
[19] H. Nakamura, T. Koga, and T. Kimura, Phys. Rev. Lett. **108**, 206601 (2012).
[20] I. E. Dzyaloshinskii, Sov. Phys. JETP **5**, 1259 (1957); T. Moriya, Phys. Rev. **120**, 91 (1960).
[21] M. Bode, E. Y. Vedmedenko, K. von Bergmann, A. Kubetzka, P. Ferriani, S. Heinze, and R. Wiesendanger, Nat. Mater. **5**, 477 (2006); M. Bode, M. Heide, K. von Bergmann, P. Ferriani, S. Heinze, G. Bihlmayer, A. Kubetzka, O. Pietzsch, S. Blügel, and R. Wiesendanger, Nature (London) **477**, 190 (2007); P. Ferriani, K. von Bergmann, E. Y. Vedmedenko, S. Heinze, M. Bode, M. Heide, G. Bihlmayer, S. Blügel, and R. Wiesendanger, Phys. Rev. Lett. **101**, 027201 (2008).
[22] M. Heide, G. Bihlmayer, and S. Blügel, Phys. Rev. B **78**, 140403 (2008); F. Schubert, Y. Mokrousov, P. Ferriani, and S. Heinze, Phys. Rev. B **83**, 165442 (2011).
[23] U. K. Rössler, A. N. Bogdanov, and C. Pfleiderer, Nature (London) **442**, 797 (2006); N. Nagaosa and Y. Tokura, Nat. Nanotechnology **8**, 899 (2013); S. Heinze, K. von Bergmann, M. Menzel, J. Brede, A. Kubetzka, R. Wiesen-

danger, G. Bihlmayer, and S. Blügel, Nat. Phys. **7**, 713 (2011).

[24] Chen, G. J. Zhu, A. Quesada, J. Li, A. T. N'Diaye, Y. Huo, T. P. Ma, Y. Chen, H. Y. Kwon, C. Won, Z. Q. Qiu, A. K. Schmid, and Y. Z. Wu, Phys. Rev. Lett. **110**, 177204 (2013); G. Chen, T. Ma, A. T. N'Diaye, H. Kwon, C. Won, Y. Wu, and A. K. Schmid, Nat. Comm. **4**, 2671 (2013).

[25] A. Thiaville, S. Rohart, E. Jué, V. Cros and A. Fert, Europhys. Lett. **100**, 57002 (2012).

[26] K. -S. Ryu, L. Thomas, S. H. Yang, and S. S. P. Parkin, Nat. Nanotech. **8**, 527 (2013); S. Emori, U. Bauer, S. -M. Ahn, E. Martinez, and G. S. D. Beach, Nat. Mater. **12**, 611 (2013).

[27] A. Brataas and K. M. D. Hals, Nat. Nanotechnology **9**, 87 (2014); A. Manchon, Nat. Phys. **10**, 340 (2014).

[28] V. M. Edelstein, S. S. Comm. **73**, 233 (1990).

[29] B. A. Bernevig and O. Vafek, Phys. Rev. B **72**, 033203 (2005); K. Obata and G. Tatara, Phys. Rev. B **77**, 214429 (2008); A. Manchon and S. Zhang, Phys. Rev. B **78**, 212405 (2008); I. Garate and A. H. MacDonald, Phys. Rev. B **80**, 214429 (2009).

[30] X. Wang and A. Manchon, Phys. Rev. Lett. **108**, 117201 (2012); E. van der Bijl and R. A. Duine, Phys. Rev. B **86**, 094406 (2012); K. -W. Kim, S. M. Seo, J. Ryu, K. -J. Lee, and H. -W. Lee, Phys. Rev. B **85**, 180404 (2012); D. A. Pesin and A. H. MacDonald, Phys. Rev. B **86**, 014416 (2012); K. M. D. Hals and A. Brataas, Phys. Rev. B **88**, 085423 (2013); C. Ortiz Pauyac, X. Wang, M. Chshiev, and A. Manchon, Appl. Phys. Lett. **102**, 252403 (2013); H. Li, X. Wang, F. Dogan, and A. Manchon, Appl. Phys. Lett. **102**, 192411 (2013); P. M. Haney, H. -W. Lee, K. -J. Lee, A. Manchon, and M. D. Stiles, Phys. Rev. B **87**, 174411 (2013).

[31] P. M. Haney, H. -W. Lee, K. -J. Lee, A. Manchon, and M. D. Stiles, Phys. Rev. B **88**, 214417 (2013); F. Freimuth, S. Blügel, and Y. Mokrousov, Phys. Rev. B **90**, 174423 (2014); G. Géranton, F. Freimuth, S. Blügel, and Y. Mokrousov, Phys. Rev. B **91**, 014417 (2015).

[32] I. M. Miron, G. Gaudin, S. Auffret, B. Rodmacq, A. Schuhl, S. Pizzini, J. Vogel, and P. Gambardella, Nat. Mat. **9**, 230 (2010); I. M. Miron, T. Moore, H. Szambolics, L. D. Buda-Prejbeanu, S. Auffret, B. Rodmacq, S. Pizzini, J. Vogel, M. Bonfim, A. Schuhl, and G. Gaudin, Nat. Mater. **10**, 419 (2011); I. M. Miron, K. Garello, G. Gaudin, P. -J. Zermatten, M. V. Costache, S. Auffret, S. Bandiera, B. Rodmacq, A. Schuhl, and P. Gambardella, Nature (London) **476**, 189 (2011).

[33] L. Liu, T. Moriyama, D. C. Ralph, and R. A. Buhrman, Phys. Rev. Lett. **106**, 036601 (2011); L. Liu, O. J. Lee, T. J. Gudmundsen, D. C. Ralph, and R. A. Buhrman, Phys. Rev. Lett. **109**, 096602 (2012); L. Liu, C. -F. Pai, Y. Li, H. W. Tseng, D. C. Ralph, and R. A. Buhrman, Science **336**, 555 (2012).

[34] D. Fang, H. Kurebayashi, J. Wunderlich, K. Výborný, L. P. Zârbo, R. P. Campion, A. Casiraghi, B. L. Gallagher, T. Jungwirth, and A. J. Ferguson, Nature Nanotech. **6**, 413 (2011); M. Jamali, K. Narayanapillai, X. Qiu, L. Ming Loong, A. Manchon, and H. Yang, Phys. Rev. Lett. **111**, 246602 (2013); J. Kim, J. Sinha, M. Hayashi, M. Yamanouchi, S. Fukami, T. Suzuki, S. Mitani, and H. Ohno, Nat. Mat. **12**, 240 (2013); X. Fan, J. Wu, Y. P. Chen, M. J. Jerry, H. W. Zhang, and J. Q. Xiao, Nat. Commun. **4**, 1799 (2013); K. Garello, I. M. Miron, C. O. Avci, F. Freimuth, Y. Mokrousov, S. Blügel, S. Auffret, O. Boulle, G. Gaudin, and P. Gambardella, Nat. Nanotech. **8**, 587 (2013); H. Kurebayashi, J. Sinova, D. Fang, A. C. Irvine, J. Wunderlich, V. Novak, R. P. Campion, B. L. Gallagher, E. K. Vehstedt, L. P. Zârbo, K. Vyborny, A. J. Ferguson, and T. Jungwirth, Nature Nanotech. **9**, 211 (2014).

[35] A. R. Mellnik, J. S. Lee, A. Richardella, J. L. Grab, P. J. Mintun, M. H. Fischer, A. Vaezi, A. Manchon, E. -A. Kim, N. Samarth, and D. C. Ralph, Nature (London) **511**, 449 (2014); Y. Fan, P. Upadhyaya, X. Kou, M. Lang, S. Takei, Z. Wang, J. Tang, L. He, L. -T. Chang, M. Montazeri, G. Yu, W. Jiang, T. Nie, R. N. Schwartz, Y. Tserkovnyak, and K. L.Wang, Nat. Mater. **13**, 699 (2014).

[36] K. -W. Kim, H. -W. Lee, K. -J. Lee, and M. D. Stiles, Phys. Rev. Lett. **111**, 216601 (2013).

[37] G. Bihlmayer, Yu. M. Koroteev, P. M. Echenique, E. V. Chulkov, and S. Blügel, Surface Science **600**, 3888 (2006).

[38] G. Bihlmayer, S. Blügel, and E. V. Chulkov, Phys. Rev. B **75**, 195414 (2007).

[39] H. Bentmann, T. Kuzumaki, G. Bihlmayer, S. Blügel, E. V. Chulkov, F. Reinert, and K. Sakamoto, Phys. Rev. B **84**, 115426 (2011).

[40] S. Grytsyuk and U. Schwingenschlögl, Phys. Rev. B, **88**, 1178 (2013).

[41] M. Montalti, A. Credi, L. Prodi, and M. T. Gandolfi, "HANDBOOK OF PHOTOCHEMISTRY", 617 (2006).

[42] J. P. Perdew, K. Burke, and M. Ernzerhof, Phys. Rev. Lett. **77**, 3865 (1996).

[43] G. Kresse and J. Furthmüller, Comput. Mater. Sci. **6**, 15 (1996).

[44] G. Kresse and D. Joubert, Phys. Rev. B **59**, 1758 (1999).

[45] url = http://www.flapw.de

[46] O. Šipr S. Bornemann, H. Ebert, S. Mankovsky, J. Vackář, and J. Minár, Phys. Rev. B **88**, 064411 (2013).

[47] A. Lehnert, S. Dennler, P. Błoński, S. Rusponi, M. Etzkorn, G. Moulas, P. Bencok, P. Gambardella, H. Brune, and J. Hafner, Phys. Rev. B **82**, 094409 (2010).

[48] S. Bornemann, O. Šipr, S. Mankovsky, S. Polesya, J. B. Staunton, W. Wurth, H. Ebert, and J. Minár, Phys. Rev. B **86**, 104436,(2012).

[49] L. Szunyogh, J. Magn. Magn. Mater. **165**, 254 (1997).

[50] B. Újfalussy, L. Szunyogh, P. Bruno, and P. Weinberger, Phys. Rev. Lett. **77**, 1805 (1996).

[51] J.-H. Park, C. H. Kim, H.-W. Lee, and J. H. Han, Phys. Rev. B **87**, 041301 (2013).

[52] S. R. Park, C. H. Kim, J. Yu, J. H. Han, and C. Kim, Phys. Rev. Lett. **107**, 156803 (2011).

[53] E. E. Krasovskii, Phys. Rev. B **90**, 115434 (2014).

[54] K. -S. Ryu, S. -H. Yang, L. Thomas, and S. S. P. Parkin, Nat. Comm. **5**, 3910 (2014).

[55] A. Varykhalov, D. Marchenko, M. R. Scholz, E. D. L. Rienks, T. K. Kim, G. Bihlmayer, J. Sánchez-Barriga, and O. Rader, Phys. Rev. Let., **108**, 066804 (2012).

[56] Certain commercial products are identified in this paper in order to specify the computational procedures adequately. Such identification is not intended to imply recommendation or endorsement by the National Institute of Standards and Technology, nor is it intended to imply that the materials or equipment identified are necessarily the best available for the purpose.